Direct Multilevel Carrier Modulation Using Millimeter-Wave Balanced Vector Modulators

Ali E. Ashtiani, Sueng-il Nam, Alex d'Espona, Stepan Lucyszyn, *Member, IEEE*, and Ian D. Robertson

***Abstract*— The importance of being able to design affordable, high-performance, millimeter-wave transmitters for digital communications and radar applications is increasing. To this end, two monolithic millimeter-wave vector modulators have been realized at 38 and 60 GHz for use in direct multilevel carrier modulation. It is shown that, by employing balanced biphase amplitude modulator elements, accurate constellations are achieved with broad-band operation from 20 to 40 GHz and 55 to 65 GHz. Modulations of 16- and 256-QAM have been demonstrated, both at 38 and 60 GHz, using this technique. Each balanced biphase amplitude modulator uses a pair of reflection-type attenuators operated in push–pull mode. This study investigates the suitability of this topology for use as a full biphase amplitude modulator for multilevel digital modulation schemes. It is found that the technique is very robust and the resulting analog vector modulator can be a very important component for many future millimeter-wave applications.**

***Index Terms*— Communications, millimeter-wave circuits, MMIC's, vector modulator.**

I. Introduction

DIRECT modulation of the carrier signal [1], [2] has been shown to be an attractive means of reducing hardware complexity and cost for wireless applications. If a conventional microwave mixer is used to upconvert the modulated signal from a low frequency to the transmission frequency, it would be impractical to filter out the unwanted sidebands at the carrier frequency. As a result, a transmitter usually requires an IF modulator followed by a complex chain of mixers, filters, and amplifiers. However, for millimeter-wave applications where cost remains a major factor restricting the widespread use of wireless systems, direct modulation is a very attractive means of realizing low-cost transmitters. Simple modulators for schemes such as amplitude-shift keying (ASK), binary phase-shift keying (BPSK), and frequency-shift keying (FSK) can be designed using a wide range of techniques. ASK modulators could employ switches, BPSK modulators could use 180° phase shifters, and FSK modulation can be achieved with either a switched voltage-controlled oscillator (VCO) or one of several small-shift frequency translation techniques available. For quadrature modulation schemes such as quaternary (or quadrature) phase-shift keying (QPSK) and quadrature amplitude modulation (QAM), an in-phase channel and quadrature-phase channel (I-Q) vector modulator is widely used [3], [4]. Recently reported direct carrier frequency modulators performances are summarized in Table I.

TABLE I
PERFORMANCE SUMMARY OF RECENTLY REPORTED DIRECT CARRIER MODULATORS

Type	Modulation	Frequency	Others
SPDT switching [5]	BPSK	1.7GHz	1^{o} phase and 0.2 dB amplitude imbalance
I-Q type with RT [8]	QPSK	8~12 GHz	$\pm 10^{o}$ phase error
I-Q type with RT [1]	QPSK	8.2 GHz	$\pm 8^{o}$ phase error
I-Q type with DBM [4]	QPSK	1~2.7 GHz	4^{o} phase imbalance
I-Q type with SBM [3]	64-QAM	5.9~8.5 GHz	$\pm 1.5^{o}$ phase error
Phase shifter/attenuator type [7]	QPSK	4~18 GHz	
Phase shifter/attenuator type [6]	QPSK	16.7~17.8 GHz	6.5 dB insertion loss
I-Q type with RT [12]	BPSK	94 GHz	$\pm 5^{o}$ phase error
I-Q type with RT ***Presented in this paper***	256 QAM, 16 QAM, QPSK	30~40 GHz and 55~65 GHz	5dB insertion loss $\pm 2^{o}$ phase error ± 0.3 dB amplitude imbalance

RT : reflection termination , DBM : Double Balanced Mixer and SBM : Single Balanced Mixer

There are two generic types of microwave vector modulators. The first is the cascaded (or α-ϕ) modulator, which simply consists of an attenuator in cascade with a phase shifter [5]. The second is the tandem modulator, which consists of a phase-splitting power-divider that creates either two or four channels, which are individually amplitude modulated and then power-combined in-phase. With the former type, which is commonly referred to as the I-Q vector modulator [6]–[8], a quadrature 3-dB power divider is used to create the two orthogonal channels. An individual biphase amplitude modulator is assigned to each channel. The output signals from these amplitude modulators are then combined using an in-phase 3-dB power combiner (e.g., a Wilkinson combiner).

With quadrature modulation schemes, it is useful to think of an M-level QAM signal as being two half-data-rate ASK signals that occupy the same bandwidth, but with an orthogonal phase relationship. A special case exists with QPSK, as it is both 4-PSK and 4-QAM. Therefore, a QPSK signal can

Manuscript received March 20, 1998; revised August 15, 1998. This work was supported by the U.K. Engineering and Physical Sciences Research Council under a collaborative project with the University of Leeds and the Queen's University of Belfast.

A. E. Ashtiani and A. d'Espona are with the Microwave Circuits and Devices Group, Department of Electronic Engineering, King's College, University of London, Strand, London WC2R 2LS, U.K. (e-mail: a.ashtiani@kcl.ac.uk).

S. Nam, S. Lucyszyn, and I. D. Robertson are with the Microwave and Systems Research Group, Department of Electronic Engineering, University of Surrey, Guildford, Surrey, GU2 5XH, U.K. (e-mail: s.lucyszyn@ee.surrey.ac.uk).

Publisher Item Identifier S 0018-9480(98)09268-0.

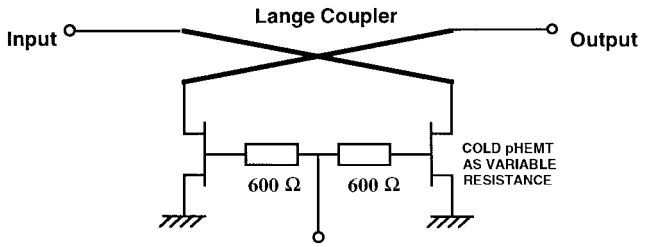

Fig. 1. Circuit topology of a direct microwave biphase amplitude modulator element.

be simply generated using two BPSK modulators. A common technique for realizing a BPSK microwave modulator is to employ a reflection topology using a Lange coupler with PIN diodes or FET's acting as switches on the coupled and direct ports, as illustrated in Fig. 1. When the switches are ON, the ideal voltage reflection coefficient is -1 (i.e., a short circuit), and when they are OFF, the ideal voltage reflection coefficient is $+1$ (i.e., an open circuit). The reflected signals add constructively at the output port only. In practice, however, at high frequencies the parasitics of the switching devices start to dominate: the series inductance and resistance in the ON-state and the shunt capacitance in the OFF-state (i.e., when the FET is biased at pinchoff). This means that the performance is far from ideal, as it suffers from both amplitude and phase errors. It is very difficult to tune out these parasitics in a wideband design.

A W-band balanced BPSK modulator employing switched amplifiers was reported by Lo *et al.* [9]. Here, a pair of amplifiers is configured in a topology similar to a balanced amplifier, employing input and output Lange couplers. However, the output is taken from the isolation port, which is normally terminated with a "dummy" load. As a result, if the amplifiers are switched ON and OFF in a push–pull mode, then a BPSK signal is generated at this isolation port. A practical drawback of this approach is that the input and output impedance matching of the amplifiers change when switched. This upsets the symmetry of the circuit and introduces amplitude and phase errors. In an expanded paper, Lo *et al.* introduced an alternative solution employing reflection-type switching elements instead of switched amplifiers [10]. Since the reflection-type circuit maintains good port matching in either state, the amplitude and phase error problem is overcome and an almost perfect response can be achieved. The natural cancellation properties of this balanced modulator ensure broad-band operation with near perfect BPSK performance, even at millimeter-wave frequencies.

For multilevel QAM, an *I-Q* vector modulator is realized employing two balanced biphase modulators operated in quadrature. Each biphase modulator has to be operated at a number of different amplitude settings (e.g., two settings for 16-QAM and eight settings for 256-QAM, each with 0° and 180° phase offset) and still needs to be operated in a push–pull mode. However, unlike the BPSK case, there is no guarantee that the constellation is perfect: while the balance of the circuit is perfect for any pair of diametrically opposite points on the constellation, it is not always the case that all the different pairs of constellation points line up together properly. So it is necessary to explain this behavior in detail by characterizing the variable resistance elements and then investigating the practical performance of the biphase amplitude modulator.

II. Cold-pHEMT Characterization

Variable resistors are found in adaptive circuits and general microwave signal processing applications. Examples include tunable active inductors [11], [12], group delay synthesizers [13], balanced modulators [6], [13], analog π-attenuators [14], and SPDT switches [15], [16]. Traditionally, current-controlled PIN diodes are used to realize a tunable resistor with hybrid MIC technology. However, due to the more expensive foundry processing and the significant control power required, PIN diodes are not often used in monolithic applications. With MMIC technology, a tunable resistor can be realized using a voltage-controlled cold-FET [6], [11]–[14], [17]. Here, no dc bias is applied to the drain termination of a standard FET. A variable voltage is applied across the gate–source terminations. With a depletion-mode FET, the depletion region expands when the negative bias voltage increases. As a result, the drain-source channel resistance increases. When the bias voltage is equal to the pinchoff voltage, the channel resistance will be very large. Ideally, the cold-FET has zero drain-source resistance at zero bias and infinite resistance at the pinchoff voltage. In practice, however, the channel resistance at zero bias is much larger than zero (due to contact and access resistances), and although a very large resistance is obtained at pinchoff, the overall impedance is dominated by the reactances of the inherent shunt capacitance.

GEC-Marconi's commercial H40 pseudomorphic HEMT process was used for this study. Here, 0.25 μm gate length AlGaAs/InGaAs pHEMT's are fabricated on 3-in diameter and 100-μm thickness wafers. Accurate modeling of cold-pHEMT's was performed using one-port S-parameter measurements of a 2×60 μm cold-pHEMT. The source termination was grounded and the reflection coefficients measured at the drain termination for gate bias points between forward bias and pinch-off. A simplified one-port equivalent circuit model for the cold-pHEMT requires only two bias dependent elements (R_P and C_P) as illustrated in Fig. 2(a). The measured and fitted values of R_P and C_P, as functions of the gate voltage V_g are shown in Fig. 2(b) and (c), respectively. A good approximation is obtained between the measured and fitted results. It can be seen that the cold-pHEMT acts predominantly as a variable resistor (having a resistance varying from 10 Ω up to 6.1 kΩ) with a small shunt capacitance (having a value varying from 50 fF down to 17 fF).

The bias-dependent R_P and C_P have been characterized using the following empirical equations:

$$\boldsymbol{R_P = a * \{b - \tanh[c(V_g + d) + e]\}} \tag{1}$$

where $a = 2800,\ b = 1.0038,\ c = 5.214,\ d = 0.4803,\ e = 2.88$.

$$\boldsymbol{C_P = a * [b + \tanh(cV_g + d)] - e} \tag{2}$$

where $a = 0.014\,954,\ b = 2.201,\ c = 2.8012,\ d = 1.925,\ e = 1.537 \times 10^{-4}$.

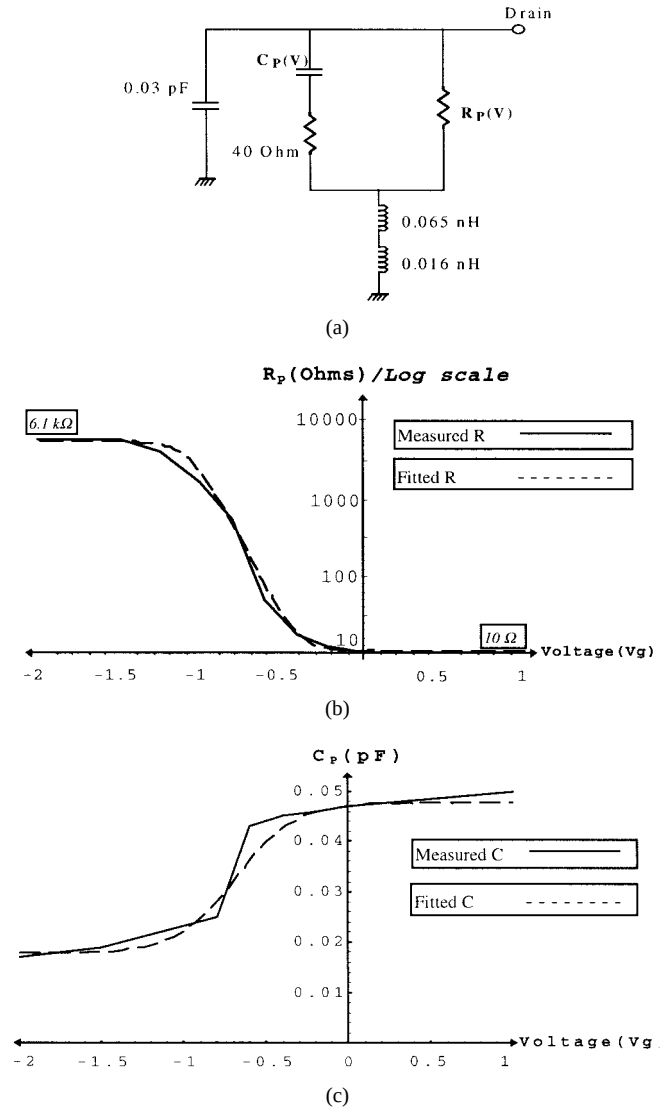

Fig. 2. (a) Equivalent circuit model of the cold-pHEMT, (b) resistance (R_P) against gate bias (V_g), (c) shunt capacitance (C_P) against gate bias (V_g).

III. Simple Modulator

The circuit topology of the simple, single-stage modulator used here is based on the well-known reflection topology, as illustrated in Fig. 1. The basic principle is that S_{11} of the reflection termination is transformed into the S_{21} of the circuit. Hence, a pure variable resistance would lead to a variable S_{21} amplitude, achieving both positive and negative signs. Therefore, $S_{21} = 0$ when the impedance of the reflection termination is set to 50 Ω. Identical reflection terminations are connected to the direct and coupled ports of the 50-Ω Lange couplers, with the other two ports forming the circuit's input and output. The incoming signal at the input port is split equally between the direct and coupled ports, with a 90° phase difference. A further 3-dB split and 90° phase difference is introduced when the waves are reflected back through the coupler. When the two reflected signals are superimposed at the input port they are in antiphase and, thus, cancel. At the isolated port of the coupler the two reflected signals are in-phase and, thus, reinforce each other to form the output signal.

For identical reflection terminations and an ideal coupler, the S-parameter matrix of the circuit is given by

$$[S] = \begin{bmatrix} 0 & -j\Gamma_T \\ -j\Gamma_T & 0 \end{bmatrix} \tag{3}$$

where $\Gamma_T =$ the voltage reflection coefficient of the reflection termination.

The resultant phase shift of the device is given by

$$\angle S_{21} = \angle \Gamma_T - 90^\circ \tag{4}.$$

It can be clearly seen from (4) how the phase shift of the circuit is dependent on Γ_T. For the parallel connection of the intrinsic resistance R_P and capacitance C_P of the cold-pHEMT, as illustrated in Fig. 2(a), the reflection coefficient is simply given by

$$\Gamma_T = \frac{Y_0 - Y_T}{Y_0 + Y_T} \tag{5}$$

where $Y_0 =$ reference admittance standard for the system ($Y_0 = 1/50\ \Omega$ in most cases)

$$Y_T = G_T + jB_T \approx (1/Rp + j\omega Cp). \tag{6}$$

Hence the reflection coefficient can be expressed as

$$\Gamma_T = \left(\frac{Y_0^2 - G_T^2 - B_T^2}{(Y_0 + G_T)^2 + B_T^2}\right) - j\left(\frac{2B_T Y_0}{(Y_0 + G_T)^2 + B_T^2}\right). \tag{7}$$

The attenuation and the phase can be obtained from

$$|\Gamma_T| = \sqrt{\left(\frac{Y_0^2 - G_T^2 - B_T^2}{(Y_0 + G_T)^2 + B_T^2}\right)^2 + \left(\frac{2B_T Y_0}{(Y_0 + G_T)^2 + B_T^2}\right)^2} \tag{8}$$

and

$$\angle \Gamma_T = \tan^{-1}\left(\frac{-2Y_0 B_T}{Y_0^2 - G_T^2 - B_T^2}\right). \tag{9}$$

The above equations clearly show that the unwanted amplitude and phase variations of the modulator will be dictated by the bias dependency of the intrinsic resistance and parasitic capacitance of the cold-pHEMT. Using these equations, a Smith's chart plot of S_{11} against bias can be determined, as illustrated in Fig. 3. It can be seen that the constellation is far from ideal, suffering from both amplitude and phase errors.

IV. Balanced Modulator

It is possible to remove the amplitude and phase errors caused by the parasitics of the pHEMT's by using a balanced modulator. The balanced modulator employs two reflection-type modulators operated in a push–pull mode [9], [10], [19], [20]. The input signal is effectively split using a balun, and the outputs from each branch, which are driven with complimentary control voltages (S and $\overline{S}$), are combined in-phase. The combined output is the vector sum of the two transmission coefficients. Since one branch is ON and the other

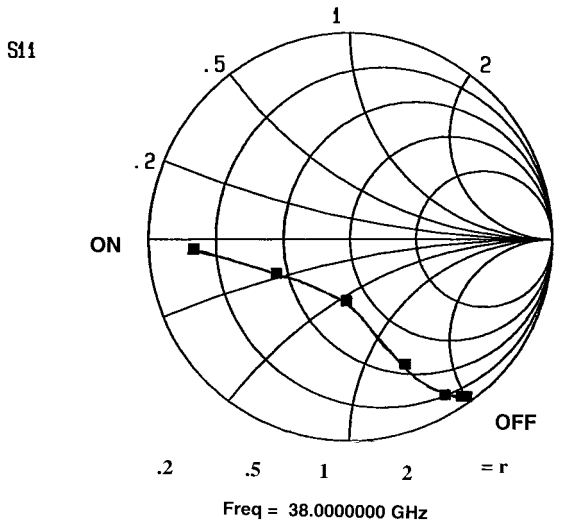

Fig. 3. S_{21} of standard single-stage reflection-type BPSK modulator using FET switches.

is OFF, or vice versa, the response is now totally symmetrical with an ideal balun, even at millimeter-wave frequencies.

Since baluns are difficult to implement in monolithic technology, it is easier to use two Lange couplers to realize the 180° operation. One coupler is placed at the input and the other at the output of an arrangement similar to a balanced amplifier, as shown in Fig. 4(a). The cold-FET reflection terminations are fed with complimentary control/baseband signals. Since Lange couplers are almost ideal, the balanced modulator gives near perfect amplitude and phase balance. The operation of this arrangement, in a BPSK mode, is illustrated in Fig. 4(b).

Using the model for the cold-pHEMT and the corresponding equations for the bias dependent elements (R_P and C_P), the reflection coefficient of each single-stage biphase amplitude modulator can be calculated using (1), (2), (6), and (7). When two such single-stage modulators are connected in tandem to form the balanced modulator, the overall voltage transmission coefficient of the circuit is given by

$$S_{21}(\text{Total}) = 0.5 * j[\Gamma_T(V_1) - \Gamma_T(V_2)] \tag{10}$$

where V_1 is the bias voltage applied to one of the single-stage modulators and V_2 is the bias voltage applied to the other single-stage modulator.

Fig. 5(a) and (b) illustrates the simulated contour plots of the attenuation and phase responses of the overall circuit, as the gate–source bias voltage of each single-stage modulator is varied from $+1$ V to -2 V. It can be seen that by moving across the dotted lines, all the possible attenuation ranges can be covered, with a phase of either $+90°$ or $-90°$.

It is possible to express S_{21} as a function of only one bias voltage by using the following empirical equation:

$$V_1 = -(1.1 + V_2). \tag{11}$$

The corresponding attenuation and phase responses of the balanced modulator, as a function of only one varying bias voltage, are illustrated in Figs. 6(a) and 7(a), respectively. The voltage wave attenuation and phase responses of the simple modulator are found using (8) and (9), and are illustrated in Figs. 6(b) and 7(b), respectively, for comparison. It can be seen that excellent performances can be achieved when using the balanced modulator. First, with reference to Figs. 6 and 7, it can be seen that 256-QAM is possible. This is because the amount of amplitude variation and tuning curve symmetry are greatly improved with the balanced approach. The resulting QAM constellation can accommodate more points. However, this is not the case with the simple modulator, as all the necessary amplitude settings cannot be covered. For example, a minimum voltage wave attenuation of $\sim 5 \times 10^{-3}$ is obtained when using the balanced modulator, compared with $\sim$0.2 for a simple modulator. More importantly, a phase shift of 180° is obtained with the balanced modulator when compared with 150° for a simple modulator. Therefore, the balance modulator can remove both amplitude and phase errors caused by the parasitics of the cold-FET's, even at millimeter-wave frequencies.

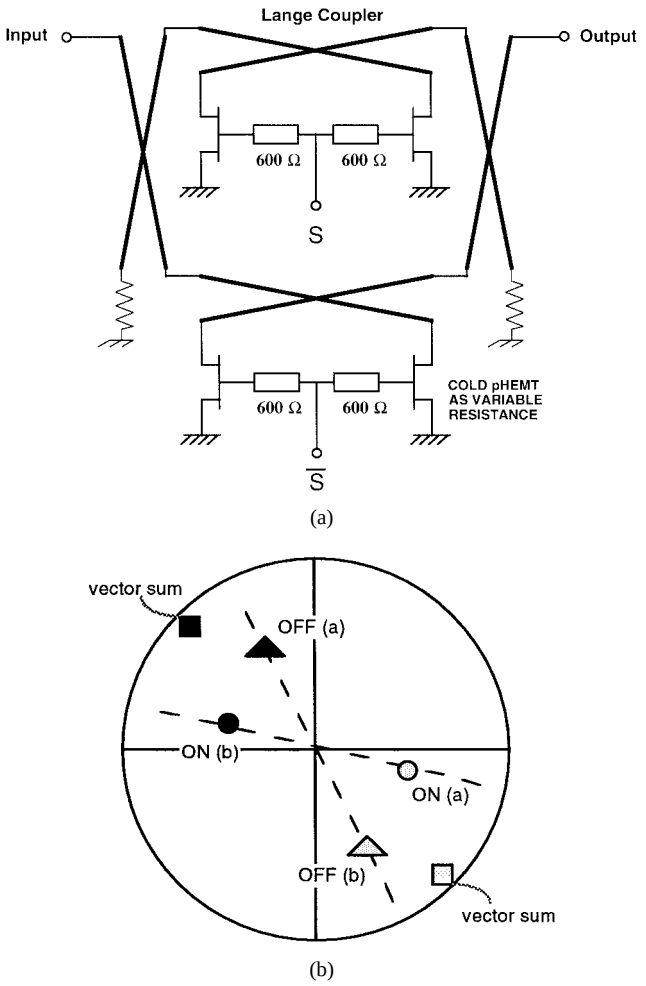

Fig. 4. (a) Balanced BPSK modulator circuit, (b) S_{21} of the modulator using balanced topology.

V. Monolithic Design and Measured Performance

The cold-pHEMT's were incorporated in the simulation using S-parameters measured on a test wafer at the Queen's University of Belfast, U.K. The other key component, the Lange coupler, was modeled by GEC-Marconi using the

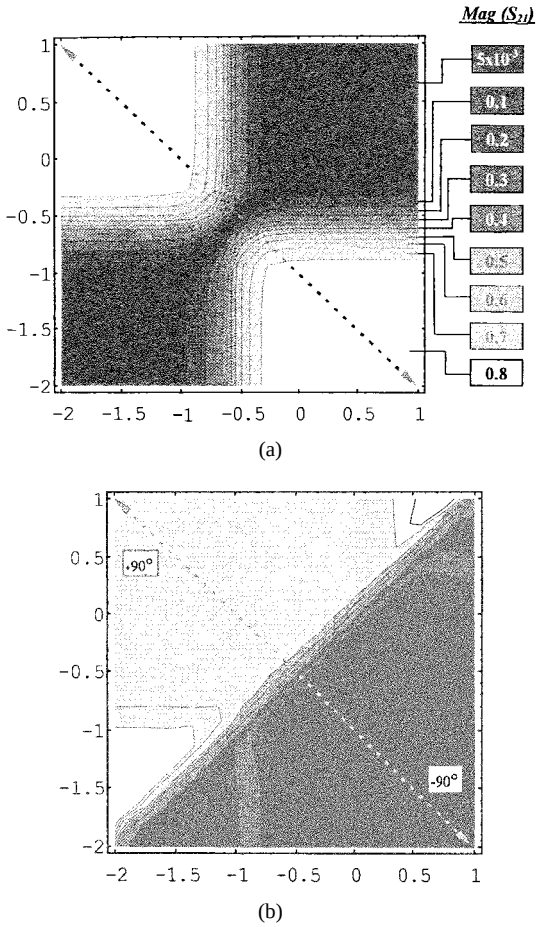

Fig. 5. Simulated contour plots of (a) attenuation and (b) phase of the overall circuit as functions of both varying bias voltages.

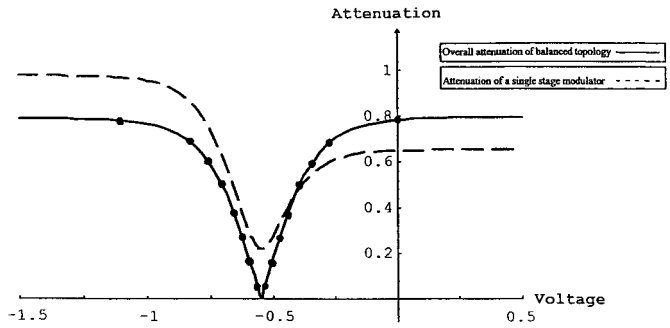

Fig. 6. Simulated attenuation as a function of one varying bias for BPSK balanced modulator (solid line) and simple modulator (dashed line).

library element in LINMIC. This was necessary in order to account for the multiple dielectrics used in the foundry process. All the other circuit elements (e.g., thin-film resistors, capacitors, microstrip lines) were modeled using *em* (by Sonnet Software), using foundry data for verification.

A microphotograph of the biphase amplitude modulator chip designed for operation at 38 GHz, which measures 1.1 × 1.5 mm^2, is shown in Fig. 8. The frequency response and static constellation were measured using a cascade on-wafer probe station and HP8510B vector network analyzer. The circuit achieved good impedance matching and with minimal amplitude and phase error over the 20–40-GHz frequency

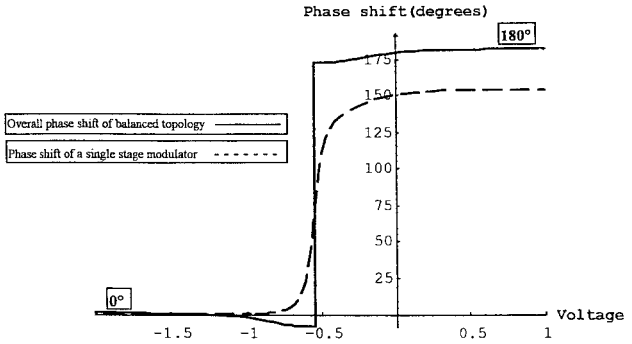

Fig. 7. Simulated phase shift as a function of one varying bias for BPSK balanced modulator (solid line) and simple modulator (dashed line).

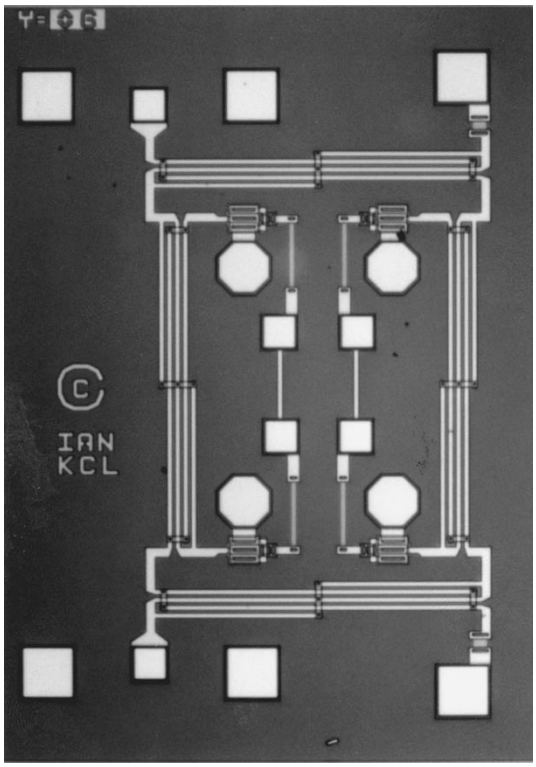

Fig. 8. Microphotograph of the 38-GHz BPSK balanced modulator.

range. Fig. 9 shows the measured performance on a polar diagram of the BPSK chip used as a bi-phase amplitude modulator. In this case, the gate bias voltages were varied from 0 to 3 V for each section individually, with the other fixed at 0 V.

For multilevel modulation schemes, the cold-pHEMT's are controlled with an analog gate–source bias voltage signal. In this way, the circuit gives a continuous range of both positive and negative transmission coefficient amplitude values and can also be used as a multifunctional I-Q vector modulator, as illustrated in Fig. 10. The vector modulator can then be used to implement multilevel digital modulation schemes such as QPSK, 16-QAM, 256-QAM, as well as used in other applications. Analog vector modulators have recently been shown to have advantages for signal processing in communications applications [21]. For example, analog control allows excellent sidelobe suppression to be achieved in digital

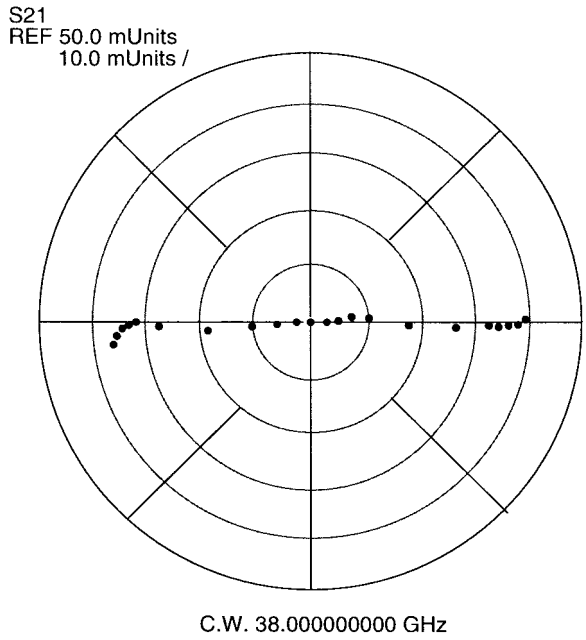

Fig. 9. Measured performance of the BPSK chip as a bi-phase amplitude modulator.

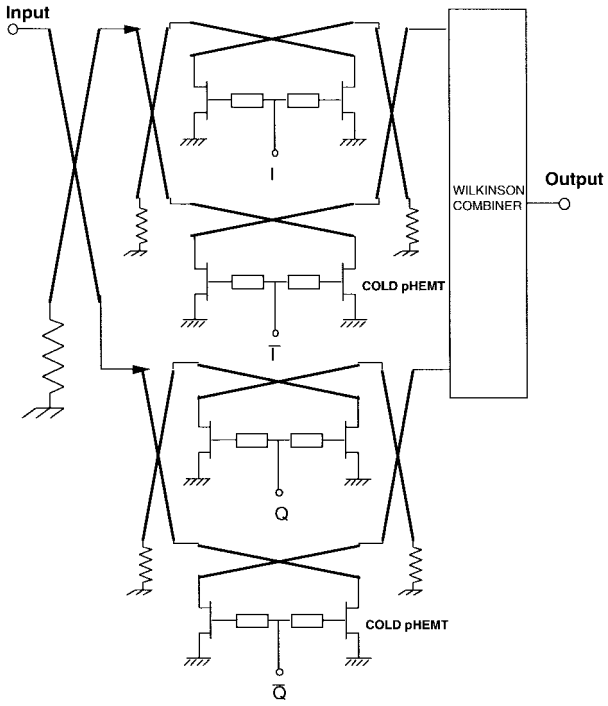

Fig. 10. Balanced vector modulator topology.

communications and can be used for performing small-shift frequency translation [22].

A. 38-GHz Vector Modulator

A microphotograph of the complete monolithic 38-GHz balanced vector modulator, which measures only 1.6×2.0 mm^2, is shown in Fig. 11. A National Instruments AT-AO-6 data-acquisition board was programmed to generate the two sets of complimentary pseudorandom sequence baseband signals: I and $\overline{I}$ and Q and $\overline{Q}$. The raw constellation measurements of the vector modulator, having no correction, can be seen in Fig. 12 for 16-QAM. For higher levels of modulation, the slight imperfections in the performance become more noticeable. For example, phase imbalance from ideal quadrature means that the constellation is not perfectly square. Fortunately, with analog control it is possible to correct these errors by careful adjustment of the I and Q signals. I and Q become interrelated, because if a constellation point is slightly southwest of its intended position, both its horizontal and vertical positions must be fine tuned. Therefore, a calibration procedure must be performed in which the I and Q voltages for each constellation point are found. These voltages are stored in a look-up table, and a digital-to-analog converter (DAC) can then be used to generate the voltages in real time. Fig. 13 shows the 256-QAM constellation at 38 GHz after a quick manual calibration was performed. The magnitude and phase performance are within ± 1 and $\pm 2\%$, respectively. Higher

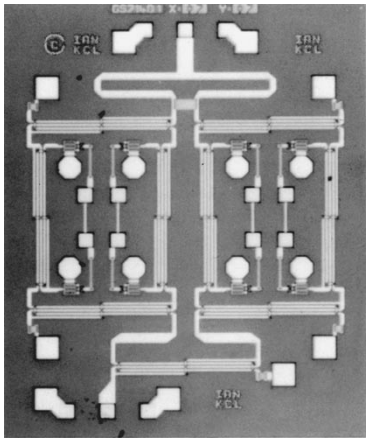

Fig. 11. Microphotograph of the complete 38-GHz balanced vector modulator.

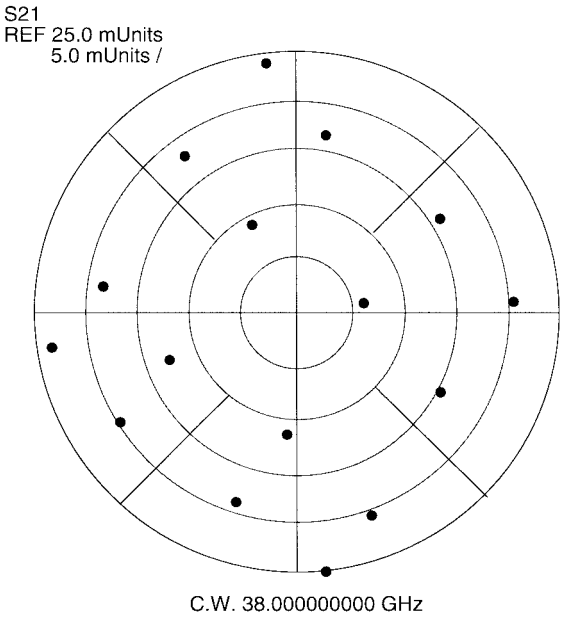

Fig. 12. Raw performance of 16-QAM vector modulator at 38 GHz.

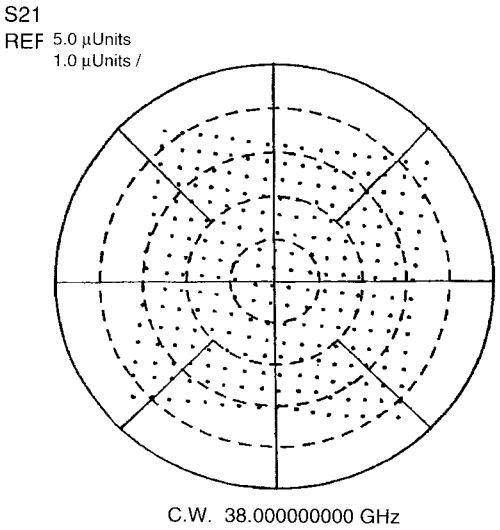

Fig. 13. Corrected performance of 256-QAM vector modulator at 38 GHz.

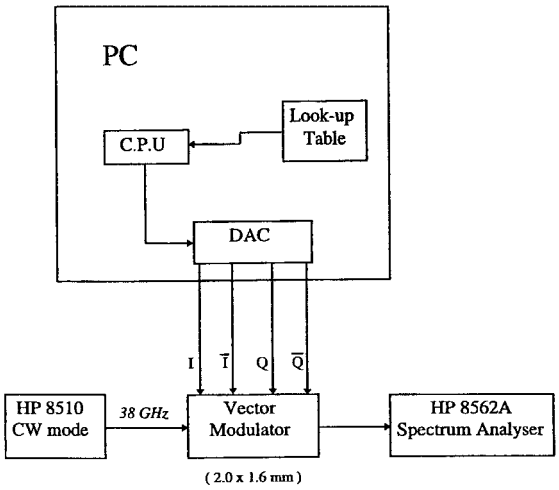

Fig. 14. Measurement setup.

accuracy and levels of modulation greater than 256-QAM (e.g., 1024-QAM) could be achieved with an automated calibration procedure. The ultimate limits being practical issues such as limited DAC precision and changes in circuit performance with temperature. In principle, both these limitations could be addressed with suitable engineering.

For the practical demonstrator presented here, a PC and DAC card were used to store the look-up table, create the pseudorandom sequence, and then generate the four analog control voltages. The measurement setup is shown in Fig. 14. The symbol rate for this configuration was limited to approximately 125 Ksymbols/s, giving an equivalent data rate of 1 Mbits/s for 256-QAM modulation. Fig. 15 illustrates the random baseband signal, which represents 16 different amplitude settings needed to achieve 256-QAM modulation. The measured output spectral response at 38 GHz is shown in Fig. 16, with no data prefiltering applied. The spectrum exhibits a textbook-style profile with deep nulls and negligible carrier breakthrough.

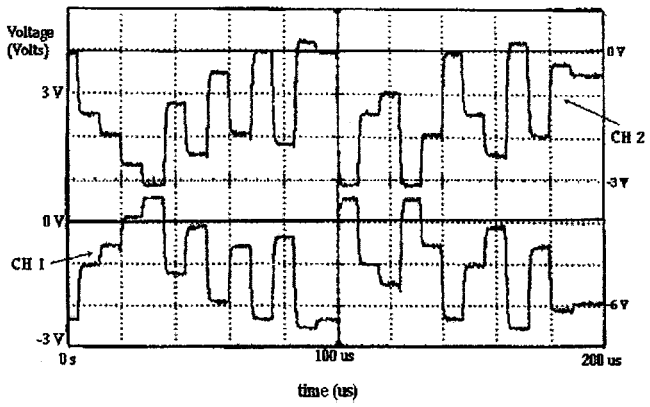

Fig. 15. Complimentary baseband signals for 256-QAM.

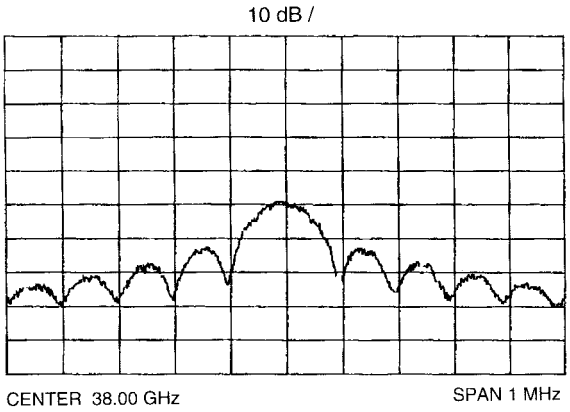

Fig. 16. Measured spectral response of the 1-Mbits/s data rate 256-QAM signal at 38 GHz.

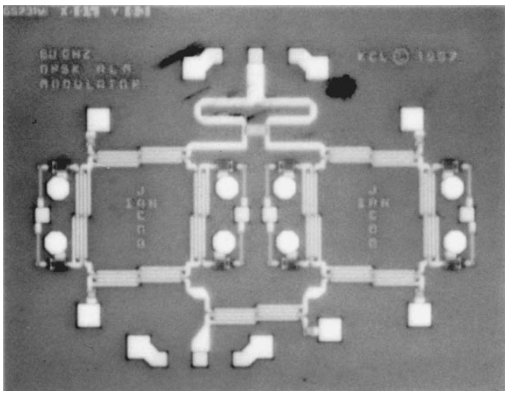

Fig. 17. Microphotograph of the complete 60-GHz balanced vector modulator.

B. 60-GHz Vector Modulator

A microphotograph of the complete monolithic 60-GHz balanced vector modulator is shown in Fig. 17. The corresponding output spectral measurement of the modulator to the same baseband signal (shown in Fig. 15) is given in Fig. 18. The symbol rate was approximately 125 Ksymbols/s, giving an equivalent data rate of 1 Mbits/s for 256-QAM modulation at the operating frequency of 60 GHz. An average insertion loss of 5 dB and worst-case input and output return loss of −10 dB have been achieved over the frequency range of 55–60 GHz,

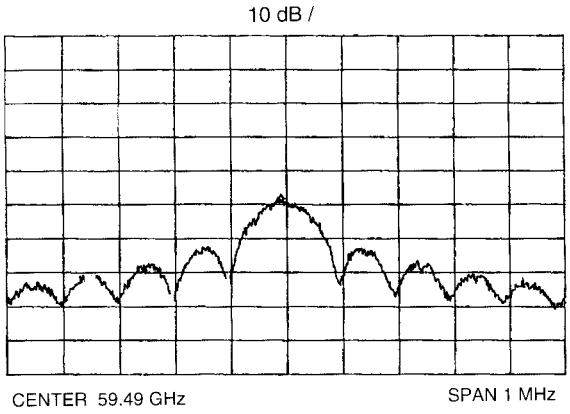

Fig. 18. Measured spectral response of the 1-Mbits/s data rate 256-QAM signal at 60 GHz.

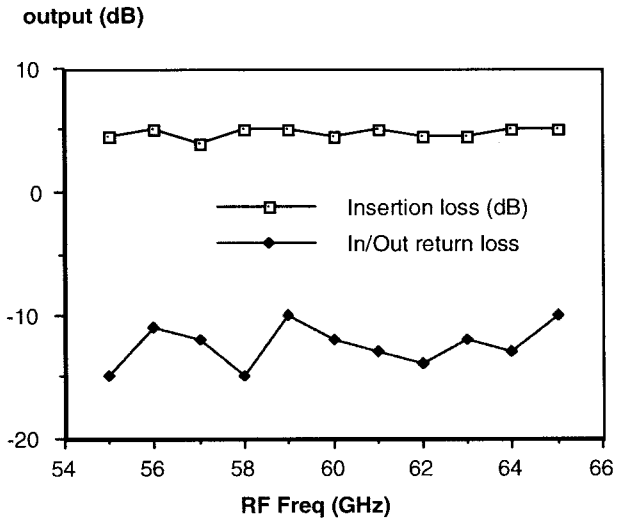

Fig. 19. Measured insertion loss and input/output return loss at 60 GHz.

as illustrated in Fig. 19. A ± 0.3 dB amplitude imbalance and $\pm 2^{\circ}$ phase error were recorded. The measured bandwidth was limited by the bandwidth of the available RF source generator. Equally good results have been achieved with BPSK, QPSK, and 16-QAM, both at 38 and 60 GHz, with a symbol rate of 200 Ksymbols/s, which is the maximum achievable with the DAC used in this study. The limited symbol rates used are not inherent to the technology presented in this study. The bit rate could be increased considerably using dedicated DSP hardware and a high-speed DAC.

VI. Conclusions

The balanced modulator using reflection-type attenuators is an extremely robust technique which gives near-perfect BPSK performance and with negligible design effort. By employing two such modulators in an I-Q modulator, near-perfect QPSK performance can be achieved. As a modulator for multilevel digital modulation, the circuit exhibits some degradation in performance with practical variable resistance elements, but with fine-tuning, excellent constellations can be achieved. Using a simple look-up table technique to calibrate the vector modulator, it has been shown that 256-QAM direct-carrier modulation can be implemented at 38 and 60 GHz with negligible hardware complexity. The 256-QAM vector modulator operating at 60 GHz is believed to be the highest multilevel modulation technique reported for the I-Q balanced vector modulator type configuration. The simplicity of the circuit topology leads to a compact chip with high yield, because the FET's are used only as variable resistance reflection terminations. In conclusion, balanced vector modulators have been shown to be very promising for implementing high-performance millimeter-wave transmitters for digital communications and radar applications.

Acknowledgment

The authors would like to acknowledge the assistance of G. Passiopoulos at King's College London and G. Green, M. Brookbanks, and A. Dearn at GEC-Marconi Materials Technology Ltd. (Caswell).

References

[1] V. Cannistraro, J.-C. Liou, and S. McCarter, "Direct modulation lowers VSAT equipment costs," *Microwaves and RF*, Aug. 1990, pp. 99–101.
[2] S. Kumar, "Directly modulated VSAT transmitters," *Microwave J.*, pp. 255–264, Apr. 1990.
[3] I. Telliez *et al.*, "A compact monolithic microwave demodulator-modulator for 64-QAM digital radio links," *IEEE Trans. Microwave Theory Tech.*, vol. 39, pp. 1947–1954, Dec. 1991.
[4] R. Pyndiah, P. Jean, R. Leblanc, and J. C. Meunier, "GaAs monolithic direct (1–2.8) GHz Q.P.S.K. modulator," in *19th European Microwave Conf. Proc.*, 1989, pp. 597–602.
[5] M. E. Goldfab *et al*., "A novel MMIC biphase modulator with variable gain using enhancement—Mode FET's suitable for 3 V wireless applications," in *IEEE MW and MM-Wave Monolithic Circuit Symp.*, 1994, pp. 99–102.
[6] S. Nam, U. Karacaoglu, C. F. O. Yerli, and I. D. Robertson, "GaAs MMIC chipset for 17/18 GHz indoor radio LAN's," in *26th European Microwave Conf. Proc.*, 1996, pp. 960–963.
[7] G. B. Norris, D. C. Boire, G. St. Onge, C. Wutke, C. Barratt, W. Coughlin, and J. Chickanosky, "A fully monolithic 4–18 GHz digital vector modulator," in *IEEE MTT-S Int. Microwave Symp. Dig.*, 1990, pp. 789–792.
[8] L. M. Devlin and B. J. Minnis, "A versatile vector modular design for MMIC," in *IEEE MTT-S Int. Microwave Symp. Dig.*, 1990, pp. 519–522.
[9] A. Truitt, J. Cerney, and J. S. Mason, "A 0.3–3 GHz monolithic vector modulator for adaptive array systems," in *IEEE MTT-S Int. Microwave Symp. Dig.*, 1989, pp. 421–422.
[10] R. Pundiah and F. V. D. Bogaart, "MMIC technology sets a new state of the art of microwave vector modulators," presented at Workshop on MMIC's for Space Applications, ESTEC, Mar. 1990.
[11] D. C. W. Lo, H. Wang, B. R. Allen, G. S. Dow, S. Chen, and M. Biedenbender, "A novel monolithic balanced switching low noise amplifier," in *IEE Microwave and Millimeter-wave Monolithic Circuits Symp. Dig.*, 1994, pp. 245–248.
[12] D. C. W. Lo, H. Wang, B. R. Allen, G. S. Dow, K. W. Chang, R. Lai, M. Biedenbender, S. Chen, and D. Yang, "Novel monolithic multifunctional balanced switching low-noise amplifiers," *IEEE Trans. Microwave Theory Tech.*, vol. 42, pp. 2629–2634, Dec. 1994.
[13] S. Lucyszyn and I. D. Robertson, "Monolithic narrow-band filter using ultrahigh-Q tunable active inductors," *IEEE Trans. Microwave Theory Tech.*, vol. 42, pp. 2617–2622, Dec. 1994.
[14] E. M. Bastida, G. P. Donzelli, and L. Scopelliti, "GaAs monolithic microwave integrated circuits using broadband tunable active inductors," in *19th European Microwave Conf. Proc.*, Sept. 1989, pp. 1282–1287.
[15] S. Lucyszyn and I. D. Robertson, "Analog reflection topology building blocks for adaptive microwave signal processing applications," *IEEE Trans. Microwave Theory Tech.*, vol. 43, pp. 601–611, Mar. 1995.
[16] R. D. Frost, D. A. Fisher, and D. E. Peck, "A GaAs MMIC voltage-controlled phase shifter," *Microwave J.*, Aug. 1991, pp. 87–94.
[17] R. Coats, J. Klein, S. D. Pritchett, and D. Zimmermann, "A low loss monolithic five-bit PIN diode phase shifter," in *IEEE MTT-S Int. Microwave Symp. Dig.*, 1990, pp. 915–918.

[18] D. Teeter, R. Wohlert, B. Cole, G. Jackson, E. Tong, P. Saledas, M. Adlerstein, M. Schindler, and S. Shanfield, "Ka-band GaAs HBT PIN diode switches and phase shifters," in *IEEE MTT-S Int. Microwave Symp. Dig.*, 1994, pp. 451–454.
[19] S. Lucyszyn, C. F. Oztec-Yerli, and I. D. Robertson, "Accurate modeling of cold-MEFETS for adaptive MMIC signal processing applications," in *25th European Microwave Conf. Proc.*, Bologna, Italy, Sept. 1995, pp. 1177–1180.
[20] H. Zirath, "Millimeter-wave mixers with focus on resistive FET-mixers," *IEEE MTT IMS Workshop Proc.* on "New developments in mixer design for microwave and millimeter-wave applications," 1996.
[21] Z. Adler and B. Smilowitz, "Octave band high precision balanced modulator," in *1984 IEEE MTT-S Dig.*, pp. 375–377.
[22] S. R. Mazumder and R. C. Waterman, "A novel 6–18 GHz 180 degree bit phase shifter configuration having very small amplitude and phase errors," in *1994 IEEE MTT-S Dig.*, pp. 83–86.
[23] S. Lucyszyn, T. Sewell, and I. D. Robertson, "Multi-level digital modulation performed directly at carrier frequency," in *25th European Microwave Conf. Proc.*, Bologna, Italy, Sept. 1995, pp. 673–676.
[24] S. Lucyszyn and I. D. Robertson, "Vector modulators for adaptive and multi-function microwave communication systems," in *Microwaves 94 Conf. Proc.*, London, U.K., Oct. 1994, pp. 103–106.

Ali E. Ashtiani was born in Tehran, Iran, on August 1, 1974. He received the Bachelors degree with honors in electronic and electrical engineering from King's College, University of London, U.K., in 1995.

He then joined the Microwave Circuits and Devices Group at King's College in 1995 as a Ph.D. student where he is currently undertaking research in the area of direct microwave modulators for low-cost millimeter-wave transmitters. He has authored/co-authored several publications in this area.

Sueng-il Nam received the B.Eng. degree in microwave engineering from Kyung-Pook National University in Korea in 1983. He received M.Sc. degree from the University of Surrey in 1993

From 1984 to 1989 he was with the System Research Centre of Hyundai Electronic Industry Ltd. where he was engaged in research on QPSK, QAM, and QPR modem implementation for single channel per carrier (SCPC) systems and very small aperture terminal (VSAT). In 1989 he joined KTI (Korea Telecom International). In 1990 he was dispatched to the University of Surrey for the KITSAT project (microsatellite development project). He subsequently joined King's College, University of London, as a Research Associate where he was carrying out research under the supervision of Dr. I. Robertson and working toward the Ph.D. degree in the same subject area. Currently, he is working with University of Surrey as a Research Fellow, U.K. His recent interests are in the MMIC implementations of transceivers for 17/18-GHz indoor radio application (MESFET), 38-GHz and 60-GHz transceiver chip set (pHEMT) for LOS communication links.

Alex d'Espona, photograph and biography not available at the time of publication.

Stepan Lucyszyn (M'91) was born in Bradford, U.K., in 1965. He received the B.Sc. degree in electronic and communication engineering from the Polytechnic of North London, London, U.K., in 1987, the M.Sc. degree in satellite communication engineering from the University of Surrey, Surrey, U.K., in 1988, and the Ph.D. degree from King's College London, London, U.K., in 1992, for his work on ultra-wide-band phase shifters for MMIC applications.

In 1989, he worked in the British and French space industries as a Junior Consultant on a broad range of projects. From 1992 to July 1995, he worked as a Post-Doctoral Research Fellow at King's College London. Since August 1995, he has been on the academic staff as Lecturer in RF Electronics at the University of Surrey. He has co-authored approximately 50 research papers in the broad area of microwave and millimeter-wave engineering for both national and international conferences and journals. In addition, he contributed three chapters to *MMIC Design* (London, U.K.: IEE, 1995). He is on the editorial board for the *International Journal of Electronics*.

Dr. Lucyszyn is a Chartered Engineer, U.K. (since 1993). He serves on the IEE Professional Group Committee E12 (Microwave Devices and Techniques). He is a member of the EPSRC Peer Review College 9 (Electronics and Photonics), serves on the editorial boards for the IEEE TRANSACTIONS ON MICROWAVE THEORY AND TECHNIQUES, and is a referee for IEEE ELECTRONICS LETTERS.

Ian D. Robertson was born in London, U.K., in 1963. He received the B.Sc. and Ph.D. degrees from King's College, University of London, London, U.K., in 1984 and 1990, respectively.

From 1984 to 1986, he was with the MMIC Research Group, Plessey Research, Caswell, U.K., where he worked on MMIC mixers, on-wafer measurement techniques, and FET characterization. From 1986 to 1998, he was with King's College, first as a Research Assistant and then as a Lecturer and Reader in microwave engineering. In 1998, he took up the Chair of Microwave Subsystems Engineering, University of Surrey, Surrey, U.K., where he currently leads an active research group in RF, microwave, and millimeter-wave circuit design and applications engineering. His research interests encompass all aspects of the design and application of MMIC's. He edited *MMIC Design* (London, U.K.: IEE, 1995).